Eur. Phys. J. C 52, 875–891 (2007)
DOI 10.1140/epjc/s10052-007-0456-7

THE EUROPEAN PHYSICAL JOURNAL C

Regular Article – Experimental Physics

Search for direct CP violating charge asymmetries in $K^{\pm} \to \pi^{\pm}\pi^{+}\pi^{-}$ and $K^{\pm} \to \pi^{\pm}\pi^{0}\pi^{0}$ decays

The NA48/2 Collaboration

J.R. Batley[1], A.J. Culling[1], G. Kalmus[1], C. Lazzeroni[1], D.J. Munday[1], M.W. Slater[1], S.A. Wotton[1], R. Arcidiacono[2], G. Bocquet[2], N. Cabibbo[2], A. Ceccucci[2], D. Cundy[2,16], V. Falaleev[2], M. Fidecaro[2], L. Gatignon[2], A. Gonidec[2], W. Kubischta[2], A. Norton[2], A. Maier[2], M. Patel[2], A. Peters[2], S. Balev[3], P.L. Frabetti[3], E. Goudzovski[3,17,a], P. Hristov[3,18], V. Kekelidze[3], V. Kozhuharov[3], L. Litov[3], D. Madigozhin[3], E. Marinova[3], N. Molokanova[3], I. Polenkevich[3], Y. Potrebenikov[3], S. Stoynev[3], A. Zinchenko[3], E. Monnier[4,19], E. Swallow[4], R. Winston[4], P. Rubin[5], A. Walker[5], W. Baldini[6], A. Cotta Ramusino[6], P. Dalpiaz[6], C. Damiani[6], M. Fiorini[6], A. Gianoli[6], M. Martini[6], F. Petrucci[6], M. Savrié[6], M. Scarpa[6], H. Wahl[6], A. Bizzeti[7,20], M. Calvetti[7], E. Celeghini[7], E. Iacopini[7], M. Lenti[7], F. Martelli[7,21], G. Ruggiero[7,17], M. Veltri[7,21], M. Behler[8], K. Eppard[8], K. Kleinknecht[8], P. Marouelli[8], L. Masetti[8,22], U. Moosbrugger[8], C. Morales Morales[8], B. Renk[8], M. Wache[8], R. Wanke[8], A. Winhart[8], D. Coward[9,22], A. Dabrowski[9], T. Fonseca Martin[9,18], M. Shieh[9], M. Szleper[9], M. Velasco[9], M.D. Wood[9,24], G. Anzivino[10], P. Cenci[10], E. Imbergamo[10], A. Nappi[10], M. Pepe[10], M.C. Petrucci[10], M. Piccini[10], M. Raggi[10], M. Valdata-Nappi[10], C. Cerri[11], G. Collazuol[11], F. Costantini[11], L. DiLella[11], N. Doble[11], R. Fantechi[11], L. Fiorini[11], S. Giudici[11], G. Lamanna[11], I. Mannelli[11], A. Michetti[11], G. Pierazzini[11], M. Sozzi[11], B. Bloch-Devaux[12], C. Cheshkov[12,18], J.B. Chèze[12], M. De Beer[12], J. Derré[12], G. Marel[12], E. Mazzucato[12], B. Peyaud[12], B. Vallage[12], M. Holder[13], M. Ziolkowski[13], S. Bifani[14], C. Biino[14], N. Cartiglia[14], M. Clemencic[14,18], S. Goy Lopez[14], F. Marchetto[14], H. Dibon[15], M. Jeitler[15], M. Markytan[15], I. Mikulec[15], G. Neuhofer[15], L. Widhalm[15]

[1] Cavendish Laboratory, University of Cambridge, Cambridge, CB3 0HE, UK[b]
[2] CERN, 1211 Genève 23, Switzerland
[3] Joint Institute for Nuclear Research, Joliot-Curie 6, 141980 Dubna, Moscow region, Russian Federation
[4] The Enrico Fermi Institute, The University of Chicago, Chicago, Illinois, 60126, USA
[5] Department of Physics and Astronomy, University of Edinburgh, JCMB King's Buildings, Mayfield Road, Edinburgh, EH9 3JZ, UK
[6] Dipartimento di Fisica dell'Università e Sezione dell'INFN di Ferrara, 44100 Ferrara, Italy
[7] Dipartimento di Fisica dell'Università e Sezione dell'INFN di Firenze, 50125 Firenze, Italy
[8] Institut für Physik, Universität Mainz, 55099 Mainz, Germany[c]
[9] Department of Physics and Astronomy, Northwestern University, Evanston, Illinois 60208-3112, USA
[10] Dipartimento di Fisica dell'Università e Sezione dell'INFN di Perugia, 06100 Perugia, Italy
[11] Dipartimento di Fisica dell'Università, Scuola Normale Superiore e Sezione dell'INFN di Pisa, 56100 Pisa, Italy
[12] DSM/DAPNIA – CEA Saclay, 91191 Gif-sur-Yvette, France
[13] Fachbereich Physik, Universität Siegen, 57068 Siegen, Germany[d]
[14] Dipartimento di Fisica Sperimentale dell'Università e Sezione dell'INFN di Torino, 10125 Torino, Italy
[15] Österreichische Akademie der Wissenschaften, Institut für Hochenergiephysik, 10560 Wien, Austria[e]
[16] Present address: Istituto di Cosmogeofisica del CNR di Torino, 10133 Torino, Italy
[17] Present address: Scuola Normale Superiore and INFN, 56100 Pisa, Italy
[18] Present address: CERN, 1211 Genève 23, Switzerland
[19] Also at Centre de Physique des Particules de Marseille, IN2P3-CNRS, Université de la Méditerranée, Marseille, France
[20] Also Istituto di Fisica, Università di Modena, 41100 Modena, Italy
[21] Istituto di Fisica, Università di Urbino, 61029 Urbino, Italy
[22] Present address: Physikalisches Institut, Universität Bonn, 53115 Bonn, Germany
[23] Permanent address: SLAC, Stanford University, Menlo Park, CA 94025, USA
[24] Present address: UCLA, Los Angeles, CA 90024, USA

Received: 12 July 2007 / Revised version: 18 September 2007 /
Published online: 1 November 2007 –

Abstract. A measurement of the direct CP violating charge asymmetries of the Dalitz plot linear slopes $A_g = (g^+ - g^-)/(g^+ + g^-)$ in $K^\pm \to \pi^\pm\pi^+\pi^-$ and $K^\pm \to \pi^\pm\pi^0\pi^0$ decays by the NA48/2 experiment at CERN SPS is presented. A new technique of asymmetry measurement involving simultaneous K^+ and K^- beams and a large data sample collected allowed a result of an unprecedented precision. The charge asymmetries were measured to be $A_g^c = (-1.5 \pm 2.2) \times 10^{-4}$ with $3.11 \times 10^9 K^\pm \to \pi^\pm\pi^+\pi^-$ decays, and $A_g^n = (1.8 \pm 1.8) \times 10^{-4}$ with $9.13 \times 10^7 K^\pm \to \pi^\pm\pi^0\pi^0$ decays. The precision of the results is limited mainly by the size of the data sample.

1 Introduction

For more than 20 years, after the discovery in 1964 that the long lived neutral kaon could decay to the same 2π final state as the short lived one [1], demonstrating that the mass eigenstates of the neutral kaons consist of a mixture of even and odd eigenstates under the combined operation of charge conjugation and parity, no other manifestation of CP violation was detected despite intensive experimental investigation. In the meanwhile the discovery of the three families of quarks and the development of the standard model (SM) made it plausible that CP violation was in fact a general property of the weak interactions, originating from a single non-trivial phase in the CKM matrix of the coefficients involved in flavour changing transitions. It was in particular realized that, barring accidental cancellations, CP violation should be relevant not only in meson–antimeson mixing but also in decays (direct CP violation) and in so called mixing induced transitions.

Two major experimental breakthroughs have since taken place. In the late 1990s, following an earlier indication by NA31 [2, 3], the NA48 and KTeV experiments firmly established the existence of direct CP violation [4–8] by measuring a non-zero value of the parameter $\mathrm{Re}(\varepsilon'/\varepsilon)$ parameter in $K^0 \to 2\pi$ decays. More recently the B-factory experiments Babar and Belle discovered a series of CP violating effects in the system of the neutral B meson [9–12].

In order to explore possible non-SM enhancements to heavy-quark loops, which are at the core of direct CP-violating processes, all possible manifestations of direct CP violation have to be studied experimentally. In kaon physics, besides the already investigated parameter $\mathrm{Re}(\varepsilon'/\varepsilon)$, the most promising complementary observables are the rates of GIM-suppressed flavour-changing neutral current decays $K \to \pi\nu\bar{\nu}$, and the charge asymmetry between K^+ and K^- decays into 3π.

It is difficult to constrain the fundamental parameters of the theory using measurements of direct CP violation in decay amplitudes due to the presence of non-perturbative hadron effects. Still, an intense theoretical programme is under way to improve predictions, aiming to allow the direct CP violation measurements to be used as quantitative constraints on the SM.

The $K^\pm \to 3\pi$ matrix element squared is conventionally parameterized [13] by a polynomial expansion[1]

$$|M(u,v)|^2 \sim 1 + gu + hu^2 + kv^2\,, \tag{1}$$

where g, h, k are the so called linear and quadratic Dalitz plot slope parameters ($|h|, |k| \ll |g|$), and the two Lorentz invariant kinematic variables u and v are defined as

$$\begin{aligned} u &= \frac{s_3 - s_0}{m_\pi^2}\,, \quad v = \frac{s_2 - s_1}{m_\pi^2}, \\ s_i &= (P_K - P_i)^2, \quad i = 1,2,3\,; \\ s_0 &= \frac{s_1 + s_2 + s_3}{3}. \end{aligned} \tag{2}$$

Here m_π is the charged pion mass, P_K and P_i are the kaon and pion four-momenta, the indices $i = 1, 2$ correspond to the two pions of the same electrical charge ("even" pions, so that v is defined up to a sign), and the index $i = 3$ to the pion of different charge (the "odd" pion). A difference between the slope parameters g^+ and g^- describing the decays of positive and negative kaons, respectively, is a manifestation of direct CP violation usually expressed by the corresponding slope asymmetry

$$A_g = (g^+ - g^-)/(g^+ + g^-) \approx \Delta g/(2g)\,, \tag{3}$$

where Δg is the slope difference and g is the average linear slope. In general terms, the slope asymmetry is expected to be strongly enhanced with respect to the asymmetry of integrated decay rates [17]. A recent full next-to-leading order ChPT computation [18] predicts A_g to be of the order of 10^{-5} within the SM. Another SM calculation [19] predicts the asymmetry in the $K^\pm \to \pi^\pm\pi^0\pi^0$ decay to be of the order of 10^{-6} (in agreement with [18] within the errors). Theoretical calculations involving processes beyond the SM [20, 21] allow a wider range of A_g, including substantial enhancements up to a few 10^{-4}.

In the past years, several experiments have searched for the CP violating slope asymmetry in both $\pi^\pm\pi^+\pi^-$ and $\pi^\pm\pi^0\pi^0$ decay modes by collecting samples of K^+ and K^- decays [22–24]. These measurements set upper

[a] e-mail: goudzovs@mail.cern.ch

[b] Funded by the U.K. Particle Physics and Astronomy Research Council

[c] Funded by the German Federal Minister for Education and Research under contract 05HK1UM1/1

[d] Funded by the German Federal Minister for Research and Technology (BMBF) under contract 056SI74

[e] Funded by the Austrian Ministry for Traffic and Research under the contract GZ 616.360/2-IV GZ 616.363/2-VIII, and by the Fonds für Wissenschaft und Forschung FWF Nr. P08929-PHY

[1] At the next order of approximation, electromagnetic interactions and final state $\pi\pi$ rescattering should be included into the decay amplitude [14–16]. These effects, despite being charge-symmetric, may still contribute to the interpretation of the results, as will be discussed below.

limits on A_g at the level of a few 10^{-3}, limited by systematic uncertainties.

The primary goal of the NA48/2 experiment at the CERN SPS is the measurement of the slope charge asymmetries A_g in both $K^{\pm} \to \pi^{\pm}\pi^{+}\pi^{-}$ and $K^{\pm} \to \pi^{\pm}\pi^{0}\pi^{0}$ processes with a sensitivity at least one order of magnitude better than previous experiments. The new level of precision can explore effects, albeit larger than the SM predictions, induced by new physics, and is achieved by using a novel measurement technique based on simultaneous K^{+} and K^{-} beams overlapping in space.

Measurements of A_g in both decay modes, performed with approximately half of the NA48/2 data sample have been published [25, 26]. This paper presents the final results, superseding these earlier results.

The plan of the paper is the following. In Sect. 2 the experimental setup is described. Section 3 contains the description of the method developed for the measurement of the slope difference which is common to both decay modes, and which aims to cancel first order systematic biases. The analyses of the $K^{\pm} \to \pi^{\pm}\pi^{+}\pi^{-}$ and $K^{\pm} \to \pi^{\pm}\pi^{0}\pi^{0}$ decay modes are discussed in Sects. 4 and 5, respectively. Discussion of the results follows in Sect. 6.

2 Beams and detectors

2.1 Simultaneous K^{+} and K^{-} beams

A high precision measurement of A_g (at the level of 10^{-4}) requires a dedicated experimental approach together with collection of very large data samples. A novel beam line providing for the first time two simultaneous charged beams of opposite signs superimposed in space over the decay fiducial volume was designed and built in the high intensity hall (ECN3) at the CERN SPS. The beam line is a key element of the experiment, as it allows decays of K^{+} and K^{-} to be recorded at the same time, and therefore leads to cancellation of several systematic uncertainties for the charge asymmetry measurement. Regular alternation of magnetic fields in all the beam line elements was adopted, which contributed to symmetrization of the average geometrical acceptance for K^{+} and K^{-} decays. The layout of the beams and detectors is shown schematically in Fig. 1.

The setup is described in a right-handed orthogonal coordinate system with the z axis directed downstream along the beam, and the y axis directed vertically up. Thus the horizontal x coordinate is such that the negative (positive) x point to the Salève (Jura) mountains. The Salève/Jura notation is used in the following analysis to denote the spectrometer magnet polarity.

The beams are produced by 400 GeV/c protons (delivered from the CERN SPS with a duty cycle of 4.8 s/16.8 s) impinging on a beryllium target of 40 cm length and 2 mm diameter. Both beams leave the target on axis at zero production angle, thereby ensuring that their source is geometrically similar and that the K^{+}/K^{-} flux ratio remains stable. It was demonstrated that the small residual difference of K^{+} and K^{-} momentum spectra produces a negligible effect on the measurement. Charged particles with momenta (60 ± 3) GeV/c are selected in a charge-symmetric way by an achromatic system of four dipole magnets with zero total deflection ('achromat'), which splits the two beams in the vertical plane and then

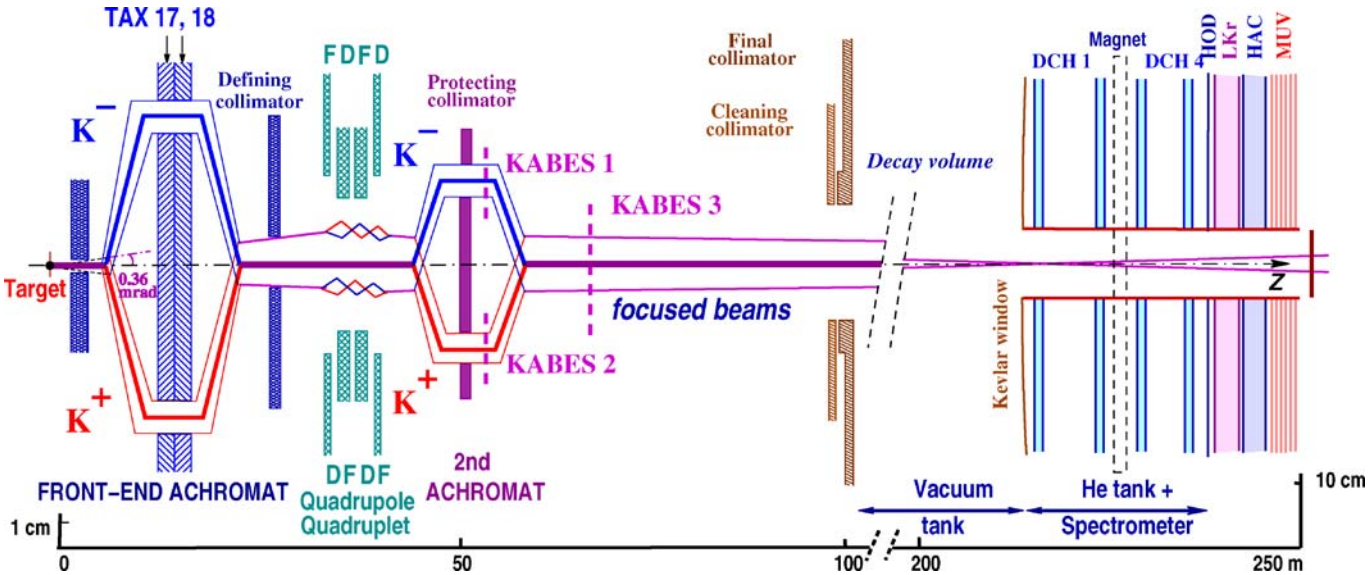

Fig. 1. Schematic side view of the NA48/2 beam line (TAX17, 18: motorized beam dump/collimators used to select the momentum of the K^{+} and K^{-} beams, FDFD/DFDF: focusing quadrupoles, KABES 1–3: kaon beam spectrometer stations), decay volume and detector (DCH 1–4: drift chambers, HOD: hodoscope, LKr: EM calorimeter, HAC: hadron calorimeter, MUV: muon veto). *Thick lines* indicate beam axes, *narrow ones* the projection of their envelopes. Note that the *vertical scales* are different in the two parts of the figure

recombines them on a common axis. Then the beams pass through a defining collimator and a series of four quadrupoles designed to produce horizontal and vertical charge-symmetric focusing of the beams towards the detector. Finally the two beams are again split in the vertical plane and recombined by a second achromat, where three stations of a Micromegas-type [27] detector operating in TPC mode form a kaon beam spectrometer KABES [28] (not used in the present analyses).

After passing through the cleaning and final collimators, the beams enter the decay volume housed in a 114 m long cylindrical vacuum tank with a diameter of 1.92 m for the first 65 m, and 2.4 m for the rest. Both beams follow the same path in the decay volume: their axes coincide to 1 mm, while their lateral sizes are about 1 cm. With 7×10^{11} protons per burst incident on the target, the positive (negative) beam flux at the entrance of the decay volume is 3.8×10^7 (2.5×10^7) particles per pulse (primarily charged pions), of which 5.7% (4.9%) are K^+ (K^-). The K^+/K^- flux ratio is about 1.8 and stable to within 1%; no correlations were observed between its variation in time and time-dependent inefficiencies of the setup. The fraction of beam kaons decaying in the decay volume at nominal momentum is 22%.

2.2 Main detectors

The decay volume is followed by a magnetic spectrometer [29] used to reconstruct tracks of charged particles. The spectrometer is housed in a tank filled with helium at nearly atmospheric pressure, separated from the vacuum tank by a thin ($0.31\%X_0$) Kevlar composite window. A thin-walled aluminium beam pipe of 16 cm outer diameter traversing the centre of the spectrometer and all the following detectors allows the undecayed beam particles and the muon halo from decays of beam pions to continue their path in vacuum. The spectrometer consists of four identical drift chambers (DCH): DCH 1, DCH 2 located upstream, and DCH 3, DCH 4 downstream of a dipole magnet. The magnet has a field integral $\int B_y \,\mathrm{d}z = 0.4\,\mathrm{Tm}$, providing a horizontal transverse momentum kick $\Delta P_x = 120\,\mathrm{MeV}/c$ for charged particles. The DCHs have the shape of a regular octagon with transverse size of about 2.8 m and fiducial area of about $4.5\,\mathrm{m}^2$. Each chamber is composed of eight planes of sense wires arranged in four pairs of staggered planes oriented horizontally, vertically, and along each of the two orthogonal 45° directions. The spatial resolution of each DCH is $\sigma_x = \sigma_y = 90\,\mu\mathrm{m}$. The nominal momentum resolution of the magnetic spectrometer is $\sigma_p/p = (1.02 \oplus 0.044 \cdot p)\%$ (p expressed in GeV/c). The measured resolution on the reconstructed $3\pi^\pm$ invariant mass varied during the data taking time in the range of $(1.65\text{–}1.72)\,\mathrm{MeV}/c^2$ in 2003 data, and $(1.76\text{–}1.82)\,\mathrm{MeV}/c^2$ in 2004, depending on DCH performance (generally, the chambers were operated at lower high voltage in 2004).

The magnetic spectrometer is followed by a plastic scintillator hodoscope (HOD) used to produce fast trigger signals and to provide precise time measurements of charged particles. The HOD, with a transverse size of about 2.4 m, consists of a plane of vertical and a plane of horizontal strip-shaped counters, each plane comprising 64 counters arranged in four quadrants. Each quadrant is logically subdivided into 4 subquadrants ("segments") which take part in the trigger logic. Counter widths (lengths) vary from 6.5 cm (121 cm) for central counters to 9.9 cm (60 cm) for peripheral ones.

The HOD is followed by a liquid krypton electromagnetic calorimeter (LKr) [30] used to detect electrons and photons. It is an almost homogeneous ionization chamber with an active volume of $7\,\mathrm{m}^3$ of liquid krypton, segmented transversally into 13248 projective cells, $2 \times 2\,\mathrm{cm}^2$ each, by a system of Cu−Be ribbon electrodes, and with no longitudinal segmentation. The calorimeter is $27X_0$ deep and has an energy resolution $\sigma(E)/E = 0.032/\sqrt{E} \oplus 0.09/E \oplus 0.0042$ (E is expressed in GeV). The spatial resolution for a single electromagnetic shower is $\sigma_x = \sigma_y = 0.42/\sqrt{E} \oplus 0.06$ cm for the transverse coordinates x and y.

The LKr is followed by a hadronic calorimeter (HAC) and a muon detector (MUV), both not used in the present analyses. A detailed description of the components of the NA48 detector can be found elsewhere [31].

2.3 Trigger logic

The event rate of $\sim 500\,\mathrm{kHz}$ is dominated by $K^\pm \to \mu^\pm\nu$ and $K^\pm \to \pi^\pm\pi^0$ decays, which are of limited physics interest as such within the NA48/2 programme. A two-level trigger system is used to select the $K^\pm \to 3\pi$ decay modes for readout, reducing the event rate to $\sim 10\,\mathrm{kHz}$.

At the first level (L1), the $K^\pm \to \pi^\pm\pi^+\pi^-$ decays are triggered by requiring coincidences of hits in the two HOD planes in at least two of the 16 segments (the L1C condition). The $K^\pm \to \pi^\pm\pi^0\pi^0$ decays are triggered by requiring a coincidence of the two HOD planes in at least one segment, and the presence of at least two distinguishable clusters of energy deposition in the LKr (the L1N condition). In some periods of data taking the L1N condition also used as input the total LKr energy deposition (see Sect. 5.4). The L1C signal is produced by the HOD logic, while the L1N signal consists of HOD and LKr components. These two components require separate analyses in order to study possible biases to the asymmetry measurement.

The second level trigger (L2) is based on a real time system computing coordinates of DCH hits using DCH drift times, and a farm of asynchronous microprocessors performing a fast reconstruction of tracks and running a decision-taking algorithm.

The L2 algorithm selecting the $K^\pm \to \pi^\pm\pi^0\pi^0$ events (L2N) examines the events passing the L1N condition, and requires the existence of a reconstructed track which, assumed to be a pion, has an energy $E^* < 230\,\mathrm{MeV}$ in the rest frame of a $K^\pm$ having a momentum of $60\,\mathrm{GeV}/c$ directed along the z axis. This condition suppresses the $K^\pm \to \pi^\pm\pi^0$ decays (which have $E^* = 248\,\mathrm{MeV}$), while keeping the $K^\pm \to \pi^\pm\pi^0\pi^0$ decays (for which E^* ranges between 140 MeV and 193 MeV).

The L2 algorithm selecting the $K^\pm \to \pi^\pm\pi^+\pi^-$ events (L2C) examines the events passing the L1C condition, and

requires at least two tracks to originate in the decay volume with the reconstructed distance of closest approach below 5 cm. L1C triggers not satisfying this condition are examined further and accepted if the L2N condition is satisfied.

NA48/2 collected data during two runs in 2003 and 2004, with ~ 50 days of efficient data taking in each run. About 18×10^9 triggers, and 200 TB of data were recorded in total.

3 The method of the slope difference measurement

3.1 Data taking strategy

Charge symmetrization of the experimental conditions is to a large extent achieved by using simultaneous superimposed K^+ and K^- beams with similar momentum spectra. However, the presence of magnetic fields in both the beam line (achromats, focusing quadrupoles, etc.) and the magnetic spectrometer, combined with some asymmetries in detector performance, introduces residual charge asymmetries. In order to equalize the local effects on the acceptance, the polarities of all the magnets in the beam transport system were reversed during the data taking on an approximately weekly basis (corresponding to the periodicity of SPS technical stops), while the polarity of the spectrometer magnet was alternated on a more frequent basis (approximately once per day in 2003 and once every 3 hours in 2004).

Data collected over a period which has all four possible setup configurations (i.e. combinations of beam line and spectrometer magnet polarities), spanning about two weeks of efficient data taking, represent a "supersample" and is treated as an independent and self-consistent set of data for the asymmetry measurement.

For the $K^\pm \to \pi^\pm\pi^+\pi^-$ analysis, nine supersamples numbered 0 to 8 were collected in two years of data taking (supersamples 0–3 in 2003 and supersamples 4–8 in 2004). For the $K^\pm \to \pi^\pm\pi^0\pi^0$ analysis, a fraction of the data sample was rejected due to poor trigger performance, and another fraction of data was merged into a larger supersample to improve the balance of magnet polarities, which resulted in seven supersamples numbered I to VII (supersamples I–III in 2003 and supersamples IV–VII in 2004).

3.2 Fitting procedure

The u-projection of the Dalitz plot is sufficient to extract the information about Δg at the desired level of precision. The measurement method is based on comparing the reconstructed u-spectra of K^+ and K^- decays (denoted as $N^+(u)$ and $N^-(u)$, respectively). In the framework of the parameterization (1), the ratio $R(u) = N^+(u)/N^-(u)$ is in good approximation proportional to

$$R(u) \sim 1 + \frac{\Delta g\, u}{1 + gu + hu^2}\,, \tag{4}$$

the contribution of the kv^2 term integrated over v being negligible. The slope difference Δg can be extracted from a fit to $R(u)$ involving the measured slope parameters g and h [13, 32], and A_g can be evaluated as in (3).

The parameters describing the Dalitz plot distribution explicitly appear in the fitting function. This generates a certain dependence of the results on the assumed shape of the event density, which in our case is (1). These effects will be discussed later.

3.3 Cancellation of systematic effects

It should be noted that any instrumental effect can induce a fake slope difference only if it is: (1) charge asymmetric and (2) correlated with u.

For a given decay mode, each supersample contains four sets of simultaneously collected $K^+ \to 3\pi$ and $K^- \to 3\pi$ samples corresponding to the four different setup configurations (eight data samples in total). To measure the charge asymmetry, exploiting the cancellations of systematic biases emerging due to polarity reversals, the following "quadruple ratio" $R_4(u)$ is evaluated. It involves the eight corresponding u spectra, and is formed by the product of four $R(u) = N^+(u)/N^-(u)$ ratios with opposite kaon sign and a deliberately chosen setup configuration in numerator and denominator:

$$R_4(u) = R_{\rm US}(u) \cdot R_{\rm UJ}(u) \cdot R_{\rm DS}(u) \cdot R_{\rm DJ}(u)\,. \tag{5}$$

Here the indices U/D denote beam line polarities corresponding to K^+ passing along the upper/lower path in the achromats of the beamline, while the indices S/J denote spectrometer magnet polarities (opposite for K^+ and K^-) corresponding to the "even" (i.e. the two identical) pions from a $K^\pm \to \pi^\pm\pi^+\pi^-$ decay being deflected to negative/positive x (i.e. towards the Salève/Jura mountains). For example, $R_{\rm US}(u)$ is the ratio of the u distribution for K^+ transported along the upper path in the beamline achromats and collected with a certain polarity of the spectrometer magnetic field, to the distribution for K^- transported along the lower path and collected with the opposite analyzing magnet polarity. A fit of the quadruple ratio (5) with a function of the form

$$f(u) = n \cdot \left(1 + \frac{\Delta g\, u}{1 + gu + hu^2}\right)^4 \tag{6}$$

results in the determination of two parameters: the normalization n and the difference of slopes Δg. The normalization is sensitive to the K^+/K^- flux ratio, while Δg is not.

The rationale for choosing the four ratios $R(u)$ appearing in (5) as the basic ones (which is not the only possibility) lies in the fact that they intrinsically cancel at first order instrumental effects linked to the imperfect left-right symmetry of the apparatus. As will be seen below, time variation of the left-right asymmetry (which is primarily due to variations of spectrometer

misalignment and beam geometry) is the largest instrumental effect, and has been the primary subject of the analysis.

The quadruple ratio technique logically completes the procedure of magnet polarity reversal, and allows a threefold cancellation of systematic biases in the data, without the need to rely on an accurate simulation of the instrumental asymmetries:

- due to spectrometer magnet polarity reversal, local detector inefficiencies cancel between K^+ and K^- samples with decay products reaching the same parts of the detector in each of the four ratios $R(u)$ appearing in the quadruple ratio $R_4(u)$;
- due to the simultaneous beams, global time-variable biases cancel between K^+ and K^- samples recorded at the same time in the product of $R_{\rm S}(u)$ and $R_{\rm J}(u)$ ratios;
- due to beam line polarity reversal, local beam line biases, resulting in slight differences in beam profiles and momentum spectra, largely cancel between the $R_{\rm U}(u)$ and $R_{\rm D}(u)$ ratios.

The method is independent of the K^+/K^- flux ratio and the relative sizes of the samples collected with different setup configurations. However, the statistical precision is limited mainly by the smallest of the samples involved, therefore the balance of sample sizes was controlled during the data taking. The result remains sensitive only to time variations of asymmetries in the experimental conditions which have a characteristic time smaller than the corresponding field alternation period.

3.4 Control quantities

In order to demonstrate that the level of cancellation of the systematic uncertainties achieved using the quadruple ratio technique is sufficient, the quantities cancelling in (5) have to be measured. For this purpose, slopes of two other control quadruple ratios built out of the eight u spectra are evaluated. These control ratios can be written as the products of the four ratios of the u spectra for same sign kaons recorded with different setup configurations. As a result, any physical asymmetry cancels in these ratios, while the setup asymmetries do not.

The fake slope difference $\Delta g_{\rm SJ}$ introduced by global time-dependent detector variations does not cancel in a ratio with opposite spectrometer polarities and identical beam line polarities in numerator and denominator, or equivalently, in the adopted notation

$$R_{\rm SJ}(u) = (R_{\rm US}(u) \cdot R_{\rm DS}(u))/(R_{\rm UJ}(u) \cdot R_{\rm DJ}(u)) \,. \qquad (7)$$

Similarly, the fake slope difference $\Delta g_{\rm UD}$ introduced by the differences of the two beam paths does not cancel in a ratio with opposite beam line polarities and identical spectrometer polarities, namely:

$$R_{\rm UD}(u) = (R_{\rm US}(u) \cdot R_{\rm UJ}(u))/(R_{\rm DS}(u) \cdot R_{\rm DJ}(u)) \,. \qquad (8)$$

It should be noted that time stability of the beam line conditions is much better than the (itself small) difference between the upper and lower beam paths.

The intrinsic left-right asymmetry of the experimental apparatus which, as already mentioned, cancels in each of the basic ratios appearing in (5), can not be directly measured by the above two control ratios (although it is accessible within an analysis based in different choice of the basic ratios). These asymmetric effects, being the largest of the residual effects and the central subject of investigation, have been taken into account with dedicated methods (see Sects. 4.2, 4.4).

Any possible systematic bias remaining in (5) is of a higher order effect than $\Delta g_{\rm SJ}$ and $\Delta g_{\rm UD}$. Thus, a measurement of fake slope differences compatible with zero, within their statistical uncertainties, validates the measurement method.

3.5 Averaging over the independent data sets

As described in Sect. 3.1, the data sample is divided into several independent self-contained supersamples. Two methods of averaging the independent results over the supersamples were considered:

- averaging the measured quadruple ratios (5) independently for each u bin, and then fitting the resulting grand quadruple ratio with the function (6);
- independent fitting of the quadruple ratios in every supersample, and then averaging the results on Δg.

The first method allows the results to be presented in a compact form, i.e. in terms of a single spectrum for each of the two decay modes. On the other hand, the second method allows a cross-check concerning several aspects of the analysis, in particular the time stability of the results.

As will be demonstrated below, the two methods lead to similar results due to the good balance of statistics which was maintained between the supersamples.

3.6 Monte Carlo simulation

Due to the method described above, no Monte Carlo (MC) corrections to the acceptance are required. Nevertheless, a detailed GEANT-based [33] MC simulation was developed as a tool for the studies of possible systematic effects; this includes full detector geometry and material description, stray magnetic fields simulation, local DCH inefficiencies, DCH misalignment, and the beam lines simulation (which allows for a reproduction of kaon momentum spectra and beam profiles). Moreover, time variations of the above effects during the running period were simulated.

A large-scale MC production was carried out for both $K^\pm \to 3\pi$ decay modes, providing samples of sizes comparable to those of the data. Namely, $\sim 10^{10}$ events were generated for each decay mode with the correct balance for each beam and detector configuration closely matching that of the data.

4 Slope difference in $K^{\pm} \to 3\pi^{\pm}$ decay

4.1 Event reconstruction and selection

Reconstruction of $K^{\pm} \to 3\pi^{\pm}$ events is based on the magnetic spectrometer information. Tracks are reconstructed from hits in DCHs using the measured magnetic field map rescaled to the recorded value of the electric current in the spectrometer analyzing magnet. Systematic uncertainties arising from this procedure due to spectrometer misalignment and imperfect knowledge of magnetic fields are discussed in Sects. 4.2 and 4.3, respectively.

Three-track vertices, compatible with the $K^{\pm} \to 3\pi^{\pm}$ decay, are reconstructed using the Kalman filter algorithm [34] by extrapolation of track segments from the upstream part of the spectrometer into the decay volume, taking into account multiple scattering in the Kevlar window and helium volume, and the stray magnetic field in the decay volume due to the Earth's field and parasitic magnetization of the vacuum tank.

The stray field is non-uniform, and has a typical magnitude of 0.5 G (comparable to the Earth field); the field map was measured in the entire vacuum tank before the 2003 run. Its effect is to induce a transverse deviation of about 1 mm and an angular deviation of about 10^{-5} rad to a 20 GeV/c charged particle traversing longitudinally the whole decay volume. Accounting for the stray field in the vertex reconstruction reduces the amplitude of the measured sinusoidal variation of the reconstructed $3\pi^{\pm}$ invariant mass with respect to the azimuthal orientation of the odd pion by more than an order of magnitude, to a level below 0.05 MeV/c^2. The event kinematics is calculated using the reconstructed track momenta and directions as extrapolated to the decay vertex.

Several stages of compaction and filtering of the data were applied, reducing the data volume from 200 TB to 1.23 TB, while reducing the number of events in the sample from 18×10^9 to 4.87×10^9. The applied filtering algorithm includes rejection of low quality data and also soft kinematic constraints: the main requirement is the presence of at least 3 reconstructed tracks in the event, which rejects about 55% of the recorded triggers.

The principal selection criteria applied to the reconstructed variables are listed below. Note that corrections to track momenta for spectrometer misalignment and magnetic field, discussed in the following Sects. 4.2 and 4.3, are applied before the kinematics of the event is reconstructed and the selection is made.

- Total charge of the three pion candidates: $Q = \pm 1$.
- Total transverse momentum with respect to the z axis: $P_{\mathrm{T}} < 0.3$ GeV/c, consistent with the angular spread of the beams and spectrometer resolution.
- Longitudinal vertex position Z_{vtx} is within the decay volume: $Z_{\mathrm{vtx}} > Z_{\mathrm{fc}}$, where Z_{fc} is the longitudinal coordinate of the final collimator of the beamline. This condition is imposed since the stray magnetic fields upstream of the final collimator have not been measured, and therefore appropriate corrections can not be made. An upper cut on Z_{vtx} is not imposed, as the geometric acceptance diminishes to zero towards the spectrometer by itself due to the presence of the beam pipe.
- Transverse decay vertex position within the beam spot: its distance from the z axis $R_{\mathrm{vtx}} < 3$ cm.
- Consistent track timing from DCHs: $|t_i - t_{\mathrm{avg}}| < 10$ ns for each track $i = 1, 2, 3$, where $t_{\mathrm{avg}} = (t_1 + t_2 + t_3)/3$, which leads to a reasonably low event pile-up probability.
- Reconstructed kaon momentum is required to be consistent with the beam momentum spectrum: 54 GeV/c $< |\mathbf{P}_K| <$ 66 GeV/c.
- Reconstructed 3π invariant mass: $|M_{3\pi} - M_K| <$ 9 MeV/c^2, where M_K is the PDG charged kaon mass [13].

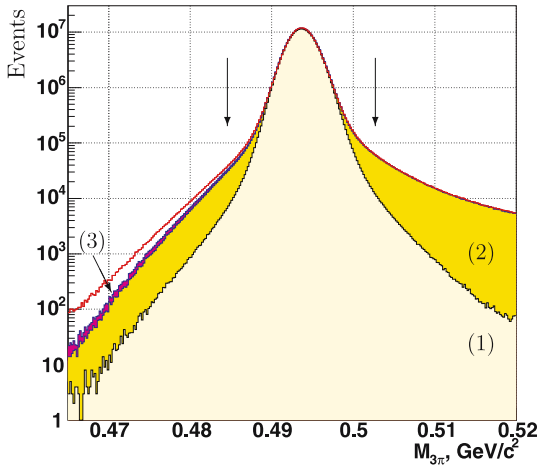

Fig. 2. Reconstructed spectrum of $3\pi^{\pm}$ invariant mass (*upper envelope curve*) and its comparison to normalized MC components: (1) events without $\pi \to \mu\nu$ decay in flight, (2) events with $\pi \to \mu\nu$ decay, (3) radiative $K_{3\pi\gamma}$ events. The selection conditions are marked with *vertical arrows*. The deficit of MC events in the low mass area is mostly outside the signal region

The distribution of the $3\pi^{\pm}$ invariant mass (before the cut on that quantity) and its comparison to MC are presented in Fig. 2. The non-Gaussian tails of the mass distribution are mainly due to $\pi^{\pm} \to \mu^{\pm}\nu_{\mu}$ decay in flight (the spectrometer reconstructing the resulting muon)[2], which is charge-symmetric. The tails are well understood in terms of MC simulation, and are considered as part of the signal. A deficit of MC events observed in the low mass region does not influence the analysis, since it is mostly outside the signal region; moreover the analysis does not rely on the MC for acceptance computation. Due to the absence of background and the presence of a non-Gaussian contribution of pion decay the selection condition for $M_{3\pi}$ corresponds to five times the resolution.

This principal stage of selection leaves a sample of 3.82×10^9 $K^{\pm} \to 3\pi^{\pm}$ events which is practically background free, as $K^{\pm} \to 3\pi^{\pm}$ is the dominant decay mode of the charged kaon with more than one charged particle in

[2] The shape and size of the non-Gaussian tails notably depend on the adopted cuts on vertex transverse position and total transverse momentum.

the final state. The fact that backgrounds due to other decays of beam kaons and pions are negligible was confirmed by a MC simulation.

4.2 Correction for spectrometer misalignment

The transverse positions of DCHs and individual wires were measured and realigned at the level of reconstruction software every 2–4 weeks of data taking using data collected during special alignment runs in which muon tracks were recorded with no magnetic field in the spectrometer. This allows an alignment precision of $\sim 30\,\mu$m to be reached. Spectrometer misalignment itself can not bias the asymmetry measurement. However, time variations of DCH alignment on a short time scale potentially can, since an uncorrected shift of a DCH along the x axis leads to charge-antisymmetric mismeasurement of the momenta.

An unambiguous measure[3] of the residual transverse horizontal misalignment is the difference between the average reconstructed 3π invariant masses corresponding to decays of K^+ and K^-, denoted as $\Delta\overline{M}$. The following sensitivities were determined from the data: a shift of the DCH 4 along the x axis by $1\,\mu$m with respect to its nominal position induces a measured mass difference of $\Delta\overline{M} = 1.4\,\mathrm{keV}/c^2$; a difference of $1\,\mu$m between the DCH 4 x-positions between the data sets taken with opposite spectrometer polarities induces a fake slope difference of $\delta(\Delta g^c) = 0.03 \times 10^{-4}$. Sensitivities to shifts of the other DCHs are similar.

Monitoring of $\Delta\overline{M}$ revealed significant transverse movements of the DCHs between the individual alignment runs, at a rate of typically below $\sim 5\,\mu$m/day and never exceeding $20\,\mu$m/day[4], which introduces spurious slope differences of the order of a few units of 10^{-5}. Introduction of time-dependent corrections to the measured momenta based on the observed $\Delta\overline{M}$ reduces these fake slope differences by more than an order of magnitude to a negligible level of $\delta(\Delta g^c) < 0.1 \times 10^{-4}$.

4.3 Effects due to spectrometer magnetic field

The measurement of pion momenta is based on the knowledge of the magnetic field in the spectrometer magnet. The variation of the current in the magnet biases the overall momentum scale of the spectrometer. This variation can be directly measured with a relative precision of 5×10^{-4}; smaller variations are continuously monitored with a precision of $\sim 10^{-5}$ using the deviation of the reconstructed charge-averaged kaon mass from the nominal PDG value [13]. A time-dependent correction can be introduced by scaling the reconstructed track momenta symmetrically for positive and negative tracks. However, the momentum scale effects are a priori highly charge-symmetric by design, due to the simultaneous K^+ and K^- beams (this was also explicitly verified by comparing the results obtained with and without the correction). Therefore no correction was applied for spectrometer current.

On the contrary, the effects caused by a non-uniform permanent (not inverting with the spectrometer magnetic field polarity) component of the magnetic field in the region of the spectrometer magnet are potentially charge asymmetric. They were studied by artificially introducing the corresponding distortions to measured track momenta depending on the coordinates of impact points in the magnetic plane, consistent with the measurement precision of the magnetic field map and the expected size of the permanent field ($\sim 1\,$G). The resulting variation of the result of $\delta(\Delta g^c) = 0.3 \times 10^{-4}$ was considered as a residual systematic uncertainty due to this effect.

Remarkably, a statistically significant Δg^c measured with the events from the side bands of $3\pi^\pm$ mass distribution (i.e. outside the signal region) can be achieved by introducing certain realistic configurations of a non-uniform permanent magnetic field in the region of the spectrometer magnet.

4.4 Correction for instability of beam geometry

The geometric acceptance for the $K^\pm \to \pi^\pm\pi^+\pi^-$ decays is mainly determined by the vacuum beam pipe traversing the centres of the DCHs, and the material in the central region of each DCH where certain groups of DCH wires terminate[5]. Moreover, the beam optics can only control the average transverse beam positions to ± 1 mm. Time variations of the transverse beam positions within the mentioned precision generate a sizable charge-asymmetric bias to the acceptance inducing instrumental slope asymmetries of the order of a few units of 10^{-4}. It would require a stability of the transverse beam positions to the level of $100\,\mu$m in order to reduce the bias to a negligible level. However it is possible to determine the average K^+ and K^- beam positions as functions of time to this order of precision and apply charge symmetric cuts, as explained below.

Inner DCH geometrical acceptance cuts which fully contain the beam pipe and the surrounding DCH regions are applied to the positions of pion impact points $\mathbf{R}_{\pi i}^{1,4}$ in the planes of DCH 1 and DCH 4 relative to the average beam intercepts in the DCH planes. These vary slightly with time and differ for K^+ and K^-.

The transverse coordinates of a beam kaon $\mathbf{R}_0^{1,2}$ in the planes of DCH 1 and DCH 2 for each event are reconstructed as the momentum-weighted averages of the coordinates $\mathbf{R}_{\pi i}^{1,2}$ of the three reconstructed pions: $\mathbf{R}_0^{1,2} = \sum_{i=1}^3 \left(\mathbf{R}_{\pi i}^{1,2}|\mathbf{P}_{\pi i}|\right) / \sum_{i=1}^3 |\mathbf{P}_{\pi i}|$, where $|\mathbf{P}_{\pi i}|$ is reconstructed momentum of a pion. Transverse coordinates of a beam kaon in the plane of DCH 4 $\mathbf{R}_0^4$ corresponding to absence of the bending by the analyzing magnet are computed by linear extrapolation using $\mathbf{R}_0^1$ and $\mathbf{R}_0^2$.

[3] Assuming CPT conservation.

[4] On an exceptional occasion during the 2003 data taking, a DCH position shifted by $200\,\mu$m in one day.

[5] Due to a relatively small Q-value of the $K^\pm \to 3\pi^\pm$ decay, $Q = 75.0\,$MeV, the outer edges of the DCHs do not bias the acceptance.

The average beam positions in the planes of DCH 1 and DCH 4 $\langle \mathbf{R}_0^{1,4} \rangle$ are computed on the basis of the distributions of $\mathbf{R}_0^1$ and $\mathbf{R}_0^4$ for the selected event sample. A bias introduced to $\langle \mathbf{R}_0^{1,4} \rangle$ by the fact that $|\mathbf{R}_{\pi i}^{1,2}|$ and $|\mathbf{P}_{\pi i}|$ are themselves affected by the acceptance is negligible. A database of the average beam positions $\langle \mathbf{R}_0^{1,4} \rangle$ depending on kaon sign, time (excursions of ~ 1 mm), kaon momentum (excursions of ~ 1 mm in the horizontal plane, ~ 1 cm in the vertical plane), and time within SPS spill (excursions of ~ 1 mm) was created.

The conditions $|\mathbf{R}_{\pi i}^{1,4} - \langle \mathbf{R}_0^{1,4} \rangle| > 11.5\,\mathrm{cm},\ i = 1,2,3$, are applied to symmetrize the beam geometry effects. These cuts cost 12% of the statistics, leading to a sample of 3.36×10^9 events. The minimum distance of 11.5 cm is chosen to ensure that the region of the beam pipe and the adjacent central insensitive areas of the DCHs are securely excluded by the cut.

The residual systematic effects arise from the stray magnetic field in the decay volume, which deflects $\mathbf{R}_{\pi i}^{1,4}$ with respect to $\langle \mathbf{R}_0^{1,4} \rangle$ in a charge-antisymmetric way. Corrections for the stray field to the measured $\mathbf{R}_0^{1,4}$ were performed. However, the precision of these corrections is limited by the precision of magnetic field measurement, which leads to a residual systematic uncertainty of $\delta(\Delta g^c) = 0.2 \times 10^{-4}$.

4.5 Correction for trigger inefficiency

Only charge-asymmetric trigger inefficiencies correlated with u can possibly bias the measurement. Inefficiencies of the individual trigger components were directly measured as functions of u using control data samples from prescaled low bias triggers collected along with the main ones. This allowed for an accounting for time variations of the efficiencies, and for a propagation of the statistical errors of the measured inefficiencies into the final result.

The trigger logic is described in Sect. 2.3. The control trigger condition for the L1 efficiency measurement requires at least one coincidence of hits in the two planes of the HOD. The control triggers for the L2 efficiency measurement are L1 triggers recorded regardless of the L2 response. The statistics of each of the two control samples is roughly 1% of the main sample[6].

The L1 trigger condition requires the coincidence of hits in two of the 16 non-overlapping HOD segments. This condition is loose as there are three charged particles in a fully reconstructed event, and the resulting inefficiency is low. It was measured to be 0.9×10^{-3} and found to be stable in time. Due to a few short-term malfunctions of a HOD channel, several subsamples of the data sample are affected by higher inefficiency (up to 7×10^{-3}), the source of the inefficiency being localized in space. This kind of inefficiency was reduced (and symmetrized) in the selected data sample by applying appropriate geometric cuts to the pion impact points on the hodoscope surface for the relevant supersamples. This procedure led to the loss of 7.1% of the statistics, reducing the final sample to 3.11×10^9 events. Due to good time stability of the L1 inefficiency, no bias from the L1 trigger is assumed. An overall uncertainty of the L1 bias was conservatively estimated to $\delta(\Delta g^c) = 0.3 \times 10^{-4}$, limited by the statistics of the control sample.

Two components of the L2 trigger inefficiency were identified: one due to trigger timing misalignment, and the other due to local DCH inefficiency (so called "geometrical"). The part related to timing misalignment has a size of $\sim 0.2\%$, and a priori does not affect the result, being uncorrelated to the kinematic variables. Its charge symmetry was checked with a detailed MC simulation of pile-up effects, and a study of the dependence of the result on the number of allowed accidental tracks. On the contrary, the geometrical part is correlated to event kinematics, and varies in time due to variations of the local DCH inefficiencies. These inefficiencies affect the trigger more than the offline reconstruction due to lower redundancy and worse online resolutions. For this reason the measured u spectra are corrected for this part of the inefficiency. The size of the inefficiency for the selected sample was measured to be close to 0.6×10^{-3}, but some periods are affected by higher inefficiency of up to 1.5% (its sources not being localized in space in a simple way). The correction to the whole statistics amounts to $\Delta(\Delta g^c) = (-0.1 \pm 0.3) \times 10^{-4}$, where the error is statistical owing to the limited size of the control sample.

The above procedure leads to over-estimation of the systematic uncertainties related to trigger inefficiencies, since the correlations of trigger inefficiencies in bins of u (in other words, smoothness of variation of trigger efficiency over u) are not taken into account.

4.6 Fits to Δg^c and cross checks

The reconstructed Dalitz plot distribution of the events passing the selection and the corrections described in the previous sections (corresponding to a fraction of the sample) is presented in Fig. 3a. Its projection to the u axis is presented in Fig. 3b[7].

The quadruple ratios of the u spectra (5) were computed, and Δg^c was measured by the two methods described in Sect. 3.5 by fitting with the function (6). The values of slope parameters $g^c = -0.21134$, $h^c = 0.01848$ recently measured by NA48/2 [32] using 55% of the 2003 data sample, and consistent with the world averages, were used. The uncertainties on the values of the above slope parameters lead to negligible effects on the result.

The grand quadruple ratio obtained by averaging quadruple ratios over supersamples in each bin of u (corrected for L2 trigger efficiency) is tabulated in Table 1, and

[6] Sizes of the control samples are adequate to measure trigger inefficiencies with a precision better that the statistical error, due to sufficiently low trigger inefficiencies.

[7] The eight u spectra corresponding to various combinations of kaon sign and magnetic field polarities involved into the computation are not presented separately, since the corresponding systematic biases are small, and the differences between the spectra are difficult to see by eye.

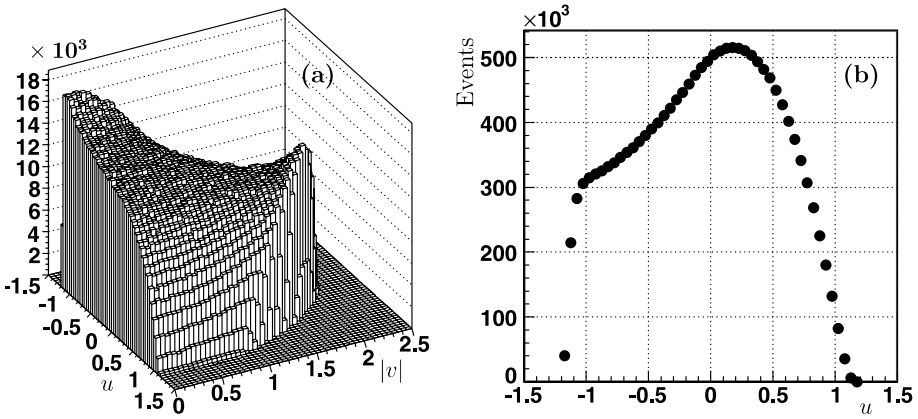

Fig. 3. a Reconstructed distribution of the selected $K^{\pm} \to \pi^{\pm}\pi^{+}\pi^{-}$ events in the kinematic variables $(u, |v|)$; **b** its projection to the u axis. The distributions correspond to a fraction of the data sample

Table 1. The quadruple ratio $R_4^c(u)$ corrected for L2 inefficiency averaged over the supersamples

u bin centre	Content	Error	u bin centre	Content	Error
−1.45	8.96034	0.52320	−0.05	10.37140	0.00730
−1.35	10.28018	0.12639	0.05	10.38555	0.00729
−1.25	10.39128	0.03900	0.15	10.37973	0.00730
−1.15	10.35639	0.01459	0.25	10.37140	0.00741
−1.05	10.38233	0.00983	0.35	10.37868	0.00755
−0.95	10.38593	0.00883	0.45	10.38286	0.00777
−0.85	10.38105	0.00855	0.55	10.36338	0.00805
−0.75	10.37476	0.00834	0.65	10.38241	0.00849
−0.65	10.38148	0.00815	0.75	10.37654	0.00907
−0.55	10.37467	0.00798	0.85	10.38572	0.00992
−0.45	10.36193	0.00780	0.95	10.40517	0.01137
−0.35	10.37647	0.00764	1.05	10.38179	0.01434
−0.25	10.37972	0.00747	1.15	10.35615	0.02568
−0.15	10.37670	0.00734	1.25	10.18942	0.25256

presented along with the result of the corresponding fit in Fig. 4.

The results of the independent fits for each supersample, including the numbers of events selected, the "raw" values of Δg^c obtained without applying the trigger corrections, and the final values of Δg^c with the L2 trigger corrections applied are presented in Table 2. The independent results obtained for the nine supersamples are shown in Fig. 5a: the individual measurements of Δg^c are statistically compatible with a $\chi^2/\mathrm{ndf} = 9.7/8$.

The measured control quantities Δg^c_{SJ} and Δg^c_{UD}, which are the slopes of the control ratios (7) and (8), for the nine supersamples are presented in Fig. 5b and c, respectively (data points are overlayed with MC ones). The sizes of these slopes induced by residual time-variable imperfections of the apparatus which cancel in the result (5) are of the same order of magnitude as the statistical errors (10^{-4}), indicating that second order effects which could induce non-zero values for them are negligible. Moreover, the comparison with MC simulations shows that the sizes of the apparatus asymmetries are well understood in terms of local inefficiencies and variations of beam optics.

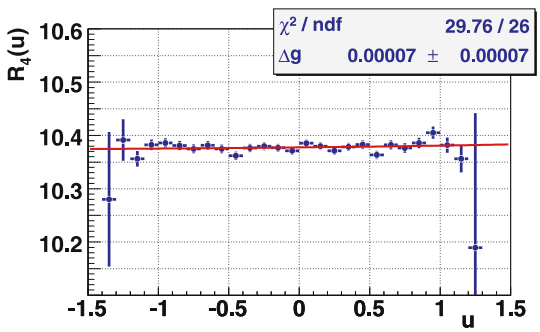

Fig. 4. The quadruple ratio $R_4^c(u)$ corrected for L2 trigger efficiency averaged in bins of u over supersamples fitted with the function (6) with $g^c = -0.21134$, $h^c = 0.01848$ [32]. The point in the first bin, given in the Table 1, is out of the vertical range

4.7 Residual systematic effects

Effects due to the difference of cross sections of π^+ and π^- hadronic interactions with the material of the detector were evaluated by a simulation of $K \to 3\pi$ decays taking into account a parameterized energy dependence of

Table 2. Statistics selected in each supersample and measured Δg^c: "raw" and corrected for L2 trigger inefficiency. The errors are statistical only; the errors in the last column include the L2 trigger efficiency errors

Supersample	$K^+ \to \pi^+\pi^+\pi^-$ decays in 10^6	$K^- \to \pi^-\pi^-\pi^+$ decays in 10^6	$\Delta g^c \times 10^4$ raw	$\Delta g^c \times 10^4$ corrected
0	448.0	249.7	0.7 ± 1.4	-0.4 ± 1.8
1	270.8	150.7	-0.8 ± 1.8	-0.8 ± 1.8
2	265.5	147.8	-1.4 ± 2.0	-1.3 ± 2.0
3	86.1	48.0	0.6 ± 3.2	1.3 ± 3.3
4	232.5	129.6	-2.7 ± 1.9	-1.6 ± 2.2
5	142.4	79.4	5.0 ± 2.5	4.8 ± 2.6
6	193.8	108.0	4.9 ± 2.1	4.9 ± 2.2
7	195.9	109.1	1.4 ± 2.1	1.3 ± 2.1
8	163.9	91.4	1.4 ± 2.3	0.5 ± 2.3
Total	1998.9	1113.7	0.8 ± 0.7	0.7 ± 0.7

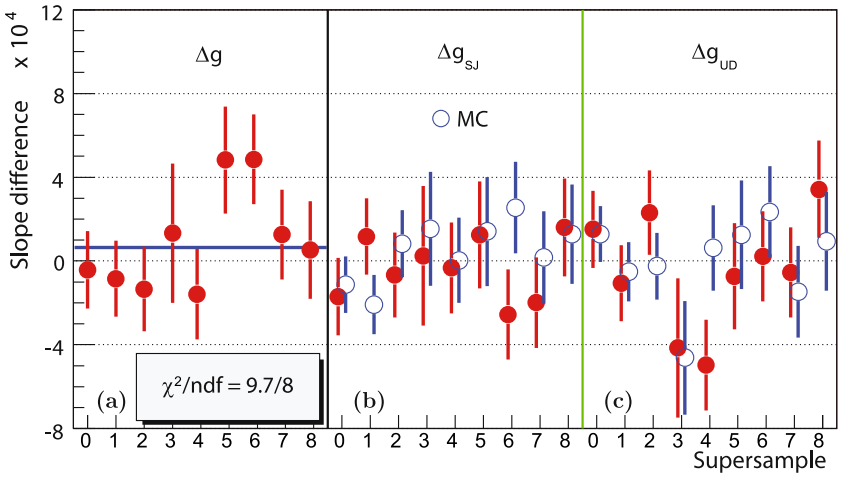

Fig. 5. **a** Δg^c measurement in the nine supersamples; control quantities **b** $\Delta g^c_{\rm SJ}$ and **c** $\Delta g^c_{\rm UD}$ corresponding to detector and beam line asymmetries which cancel in the quadruple ratio, and their comparison to MC (*open circles*)

cross sections of $\pi^\pm N$ interactions [13, 35] and the material composition of the detector. As the most striking example of the effect of the charge asymmetry of $\pi^\pm N$ cross sections, a $\pi^- p$ interaction in the first plastic scintillator plane of the HOD, giving rise to a fully neutral final state, produces a trigger bias for $K^- \to \pi^-\pi^0\pi^0$ decays relative to $K^+ \to \pi^+\pi^0\pi^-$ decays. Owing to the kaon momentum spectrum, $\pi^\pm$ momentum in the detector is restricted to $p_\pi > 5$ GeV/c, which 1) validates the use of the cross section parameterization, and 2) makes the measurement insensitive to the largest differences between $\pi^+ p$ and $\pi^- p$ cross sections occurring at $p_\pi \sim 1$ GeV/c. The integral charge-asymmetric effects were found to be of the order of 10^{-4}, however their u-dependence was found to be negligible, inducing a bias of only the order of $\Delta g \sim 10^{-6}$.

The effects due to the difference of K^+ and K^- production spectra by the primary protons [36] do not cancel in the quadruple ratio. The difference between the K^+ and K^- spectra was quantified by measuring the slope of the quadruple ratio of the reconstructed K^+ and K^- momentum spectra. The slope of the K^+/K^- spectra ratio $f(p)$ normalized by $f(60\,\text{GeV}) = 1$ was determined to be $\mathrm{d}f(p)/\mathrm{d}p = 0.6\%/(\text{GeV}/c)$. This induces charge asymmetry of geometrical acceptance leading to a fake slope difference of $\delta(\Delta g^c) = 0.3 \times 10^{-3}$, as estimated by a MC simulation. This value was conservatively taken as the corresponding systematic uncertainty.

Taking into account that the composition of the beams is not charge symmetric (in particular, the K^+ and K^- fluxes differ), event distortions caused by pile-up with the products of another kaon decay or a beam halo particle traversing the sensitive region of the spectrometer is a potential source of systematic bias. To study the pile-up effects an accidental activity generator was introduced into the MC. This generator was tuned using the measured composition of beam and halo fluxes, and a production of $\sim 10^8$ correlated pairs of an original kaon decay event and a piled-up event was carried out. No charge-asymmetric effects were observed in the reconstructed u distributions nor in the L2 trigger inefficiencies down to a level of $\delta(\Delta g^c) = 0.2 \times 10^{-4}$, limited by MC statistics.

Biases due to resolution effects were studied by using various methods of expressing the u variable in terms of directly measured quantities (using only the invariant mass of the pair of even pions in the laboratory frame; using the energy of the odd pion in the kaon rest frame; using a 3C kinematic fit constraining kaon mass and direction) differing in resolution as a function of u. Stability of the

Table 3. Systematic uncertainties and the correction for L2 trigger inefficiency for Δg^c measurement

Systematic effect	Correction, uncertainty $\delta(\Delta g^c) \times 10^4$
Spectrometer misalignment	± 0.1
Spectrometer magnetic field	± 0.3
Beam geometry and stray magnetic fields	± 0.2
Kaon production spectra	± 0.3
Pile-up	± 0.2
Resolution and fitting	± 0.2
Total purely systematic uncertainty	± 0.6
L1 trigger inefficiency	± 0.3
L2 trigger inefficiency	-0.1 ± 0.3

result with respect to variation of bin size in u has been studied as well. An estimate for the systematic uncertainty due to resolution effects of $\delta(\Delta g^c) = 0.2 \times 10^{-4}$ has been obtained.

4.8 The resulting A_g^c

A summary of the systematic uncertainties, including a correction for L2 trigger inefficiency, is presented in Table 3. The difference in the linear slope parameter of the Dalitz plot of the $K^\pm \to \pi^\pm\pi^+\pi^-$ decays, measured with the full NA48/2 data sample of 3.11×10^9 events, is found to be

$$\Delta g^c = g^+ - g^- = (0.7 \pm 0.7_{\text{stat.}} \pm 0.4_{\text{trig.}} \pm 0.6_{\text{syst.}}) \times 10^{-4}. \quad (9)$$

Here the individual systematic errors are added in quadrature, and the errors due to trigger inefficiencies are of statistical nature. Converted to the direct CP violating charge asymmetry (3) using the value of the Dalitz plot slope $g^c = -0.21134 \pm 0.00017$ recently measured by the NA48/2 [32],

$$\begin{aligned} A_g^c &= (-1.5 \pm 1.5_{\text{stat.}} \pm 0.9_{\text{trig.}} \pm 1.3_{\text{syst.}}) \times 10^{-4} \\ &= (-1.5 \pm 2.2) \times 10^{-4}. \end{aligned} \quad (10)$$

5 Slope difference in $K^\pm \to \pi^\pm\pi^0\pi^0$ decay

5.1 Event reconstruction and selection

The $K^\pm \to \pi^\pm\pi^0\pi^0$ decays are reconstructed considering $\pi^0 \to \gamma\gamma$ decays of each of the π^0s and hence the reconstruction of the four photons is required. The principal selection criteria are described below.

– An energy deposition cluster in the LKr is considered to correspond to a photon candidate if the following conditions are fulfilled: 1) it has an energy $E >$ 3 GeV, which minimizes effects of nonlinearity of the LKr response (typically 2% at 3 GeV and becoming negligible above 10 GeV); 2) it is situated at distances larger than 10 cm from other clusters, and at distances larger than 15 cm from impact points of the reconstructed charged particles, which minimizes effects of energy sharing between the reconstructed clusters due to overlap; 3) it satisfies requirements on distances from the outer LKr edges and the beam pipe, which ensures full lateral containment of the electromagnetic showers.
– The event is required to have at least one reconstructed track of a charged particle, and at least four photon candidates.
– To suppress the charge-asymmetric DCH acceptance bias induced by the time instability of beam geometry, cuts are applied to distances between the track impact points in DCH 1 and DCH 4 planes $\mathbf{R}_\pi^{1,4}$ and the average reconstructed beam positions $\langle \mathbf{R}_0^{1,4} \rangle$. These cuts are similar to those applied in the $K^\pm \to \pi^\pm\pi^+\pi^-$ analysis; the rationale and a description are contained in Sect. 4.4.

For each selected event, a $K^\pm \to \pi^\pm\pi^0\pi^0$ decay is reconstructed as follows. Assuming that a pair of photon candidates i, j $(i, j = 1, 2, 3, 4)$ originates from a $\pi^0 \to \gamma\gamma$ decay occurring at a distance D_{ij} from the LKr front face, then D_{ij} is calculated to very good approximation as $D_{ij} = R_{ij}\sqrt{E_i E_j}/m_{\pi^0}$, where E_i and E_j are the energies of the i-th and j-th photon candidates, R_{ij} is the distance between their impact points at the LKr front plane, and m_{π^0} is the PDG π^0 mass [13].

To search for two $\pi^0 \to \gamma\gamma$ decays occurring at the same point of the decay volume, among all the combinations of non-overlapping photon candidate pairs (i, j) and (k, l) the one with the smallest value of $|D_{ij} - D_{kl}|$ is selected. Moreover, the smallest of $|D_{ij} - D_{kl}|$ is required to be less than 500 cm, while the resolution on the difference $D_{ij} - D_{kl}$ for photon pairs originating from the same point of space is ~ 100 cm. For the best selected (if any) combination (i, j) and (k, l), the value of $(D_{ij} + D_{kl})/2$ is used to define the longitudinal position of a $K^\pm$ decay vertex Z_{vtx}.

No geometrical information about the $\pi^\pm$ track is used for vertex reconstruction in order to avoid the related charge-asymmetric biases induced by beam geometry variation and stray magnetic fields.

The following selection criteria are applied to the reconstructed event kinematics.

– The longitudinal vertex position required to be within the decay volume: $Z_{\text{vtx}} > Z_{\text{fc}}$, where Z_{fc} is the longitudinal coordinate of the final collimator.
– Consistent photon and track timing: $|t^\gamma_{\text{avg}} - t^\gamma_i| < 5$, $|t^\gamma_{\text{avg}} - t^\pm| < 20$ ns, where t^γ_i are times of the four selected LKr clusters, $t^\pm$ is the time of the selected track, and $t^\gamma_{\text{avg}} = \sum t^\gamma_i/4$.
– Reconstructed kaon momentum is required to be consistent with the beam momentum spectrum: $54\,\text{GeV}/c < |\mathbf{P}_K| < 66\,\text{GeV}/c$.

– Reconstructed 3π invariant mass: $|M_{3\pi} - M_K| < 6\,\mathrm{MeV}/c^2$. This cut is narrower than in the $K^\pm \to 3\pi^\pm$ case due to a better mass resolution.

The above requirements lead to the final sample of 9.13×10^7 events. Figure 6 shows the $\pi^\pm\pi^0\pi^0$ invariant mass distribution (before a cut on this quantity). The resolution on the invariant mass is $0.9\,\mathrm{MeV}/c^2$. The tails of the mass distribution originate from wrong photon pairing (the fraction of these events estimated by a MC simulation is 0.2%) and $\pi \to \mu\nu$ decays. The background is negligible for the applied mass cut.

It can be seen from (2) that the kinematic variable u can be computed using only the $\pi^0\pi^0$ invariant mass. Thus a measurement of u uses the information from the LKr only, not involving the DCH data. This provides a certain charge symmetry of the procedure, as the LKr is a "charge blind" subdetector, except for effects of small differences between π^+ and π^- interaction characteristics.

The reconstructed Dalitz plot distribution of the selected events is shown in Fig. 7a, and its projection on the u axis is presented in Fig. 7b.

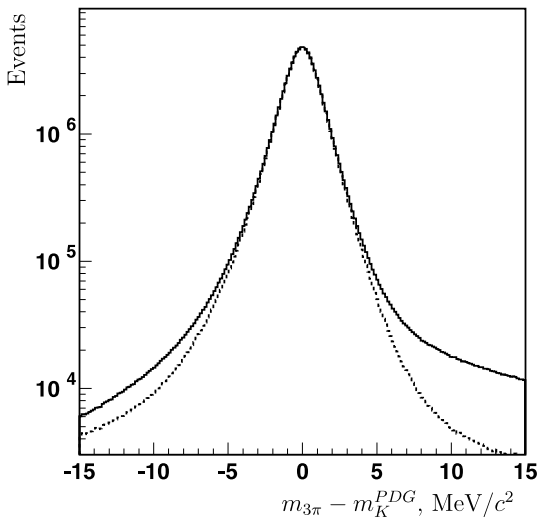

Fig. 6. Deviation of the reconstructed $\pi^\pm\pi^0\pi^0$ invariant mass from the PDG kaon mass [13]. The *dashed histogram* shows the same distribution for events with no hits in the muon detector (not used in the analysis)

5.2 Fits to Δg^n and cross checks

Quadruple ratios of the u spectra (5) were computed, and Δg^n was measured by the two methods described in Sect. 3.5 involving fitting with the function (6). The nominal values of slope parameters $g^n = 0.626$, $h^n = 0.052$ [13] were used. Unlike the $K^\pm \to \pi^\pm\pi^+\pi^-$ case, no trigger corrections to the u spectra are required, as discussed in Sect. 5.4.

A grand quadruple ratio obtained by averaging quadruple ratios over supersamples in every bin of u is tabulated in Table 4, and presented along with the result of the corresponding fit in Fig. 8.

Numbers of selected events and the results of the fits in every supersample are presented in Table 5. The independent results obtained in the seven supersamples are shown in Fig. 9a: the individual measurements are compatible with a $\chi^2/\mathrm{ndf} = 1.5/6$.

The measured control quantities Δg^n_{SJ} and Δg^n_{UD}, which are the slopes of the control ratios (7) and (8), in the seven supersamples are presented in Fig. 9b and c, respectively (data points are overlayed with MC ones). These instrumental asymmetries do not exceed the size of the statistical errors, and are well reproduced by the MC simulation.

5.3 Systematic effects due to calorimeter performance

As discussed above, the LKr calorimeter is the primary detector for $K^\pm \to \pi^\pm\pi^0\pi^0$ decay reconstruction, and the only detector used for measurement of the variable u. The

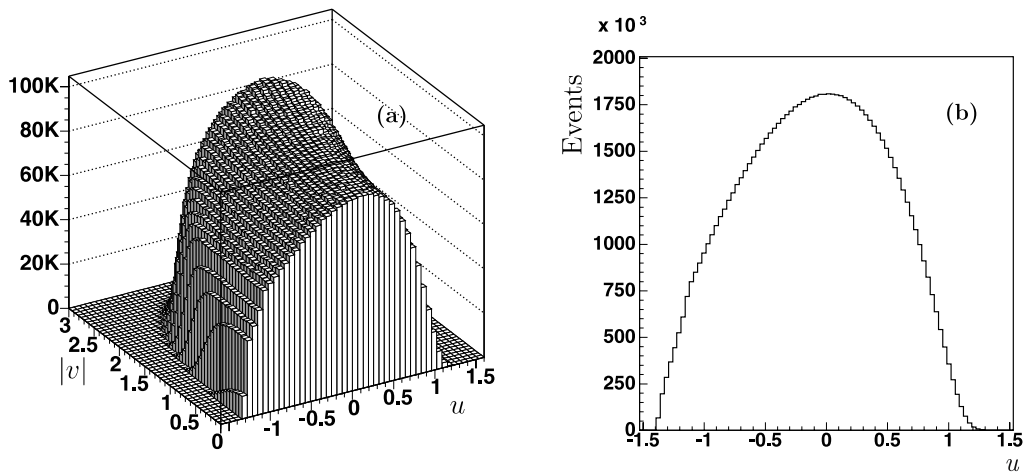

Fig. 7. a Reconstructed Dalitz plot distribution in the kinematic variables $(u,|v|)$ for the selected $K^\pm \to \pi^\pm\pi^0\pi^0$ events; **b** u-spectrum for the selected events

Table 4. The quadruple ratio $R_4^n(u)$ averaged over supersamples

u bin centre	Content	Error	u bin centre	Content	Error
−1.35	10.2110	0.1248	0.05	10.4213	0.0381
−1.25	10.2762	0.0775	0.15	10.3864	0.0382
−1.15	10.4234	0.0621	0.25	10.4363	0.0389
−1.05	10.5216	0.0552	0.35	10.3485	0.0393
−0.95	10.4020	0.0504	0.45	10.4804	0.0411
−0.85	10.4261	0.0474	0.55	10.4494	0.0430
−0.75	10.3868	0.0449	0.65	10.4222	0.0458
−0.65	10.4322	0.0432	0.75	10.4725	0.0507
−0.55	10.3885	0.0415	0.85	10.4576	0.0584
−0.45	10.3781	0.0403	0.95	10.4599	0.0726
−0.35	10.4039	0.0395	1.05	10.3386	0.1028
−0.25	10.3408	0.0386	1.15	10.1208	0.1912
−0.15	10.4057	0.0383	1.25	10.1472	0.5851
−0.05	10.4262	0.0382	1.35	8.8335	2.7018

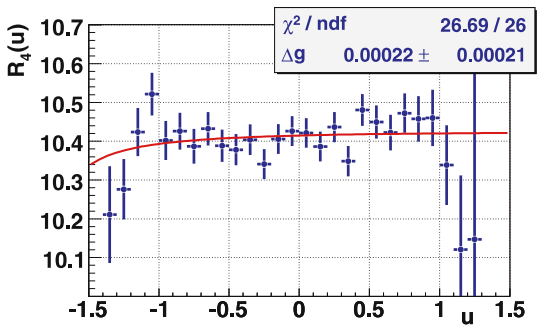

Fig. 8. The quadruple ratio $R_4^n(u)$ averaged by supersamples in bins of u fitted with the function (6) with $g^n = 0.626$, $h^n = 0.052$ [13]

Table 5. Selected statistics and measured Δg^n in each supersample

Supersample	$K^+ \to \pi^+\pi^0\pi^0$ decays in 10^6	$K^- \to \pi^-\pi^0\pi^0$ decays in 10^6	$\Delta g^n \times 10^4$
I	16.40	9.14	3.4 ± 3.9
II	10.17	5.66	0.6 ± 5.1
III	3.71	2.06	-3.0 ± 8.4
IV	5.15	2.87	4.8 ± 7.1
V	8.88	4.94	4.1 ± 5.3
VI	7.49	4.17	4.1 ± 5.8
VII	6.86	3.82	-2.1 ± 6.0
Total	58.66	32.66	2.2 ± 2.1

only charge-asymmetric effect in LKr performance is related to the difference between π^+ and π^- interaction cross sections. Variation of the cut on the minimum allowed distance between the photon candidate clusters and the impact point of the charged track on LKr front face led to a conservative estimation of the corresponding systematic uncertainty: $\delta(\Delta g^n) = 0.5 \times 10^{-4}$. Introduction of a shower energy sharing correction leads to a consistent estimate.

Other effects related to the LKr reconstruction are not expected to induce fake charge asymmetries. However the following stability checks were performed.

- Stability with respect to variation of the resolution on the reconstructed u variable for K^+ and K^- decays was studied with a large sample of events simulated by MC. The result was found to be stable within 0.1×10^{-4}.
- The result is stable to 0.1×10^{-4} with respect to introducing various ways of correcting the measured photon energies to account for nonlinearity of the LKr response at low energy.
- The effect of wrong photon pairing in the reconstruction of the $\pi^0\pi^0$ pair was studied by a large sample of simulated events. The result was found stable to better than 0.1×10^{-4}.
- The result was found to have negligible sensitivy to variation of the cluster radial distance cut value around the beam pipe.

5.4 Uncertainties due to trigger inefficiency

The trigger logic is described in Sect. 2.3. Charge symmetry of every trigger component was studied either by direct measurement using samples recorded with low bias control triggers, or by simulation, as discussed below.

The inefficiency of the HOD component of the L1N trigger, which is due to inefficiency of the HOD counters, was measured using a control sample of all events with exactly one reconstructed track, triggered by conditions requiring activity in the LKr. The integral inefficiency for the selected $K^\pm \to \pi^\pm\pi^0\pi^0$ sample was measured to be about 0.25%. It increased up to 2.0% during short periods due to malfunctioning of a few HOD counters; this effect was reduced and symmetrized, as described in Sect. 4.5. The measured map of inefficiency measured as a function of the (x, y) coordinates at the HOD plane allowed a precise estimation of trigger inefficiency effect to be made. It was found to be consistent with no spurious asymmetry at the level of $\delta(\Delta g^n) = 0.1 \times 10^{-4}$.

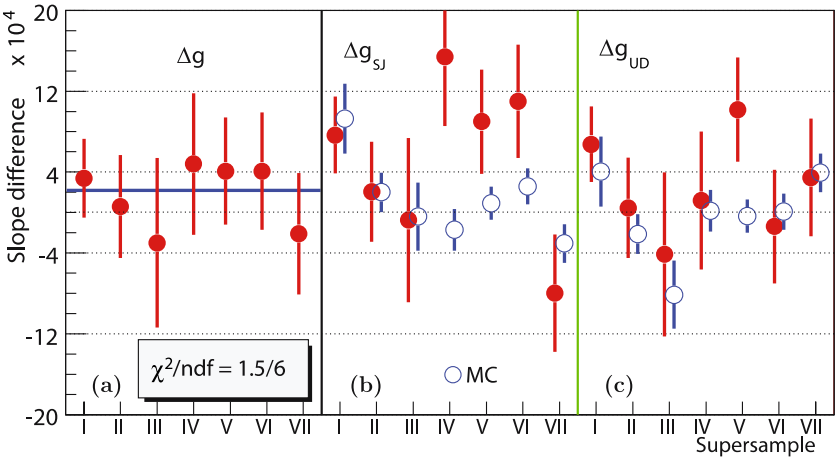

Fig. 9. **a** Δg^n measurement in the seven supersamples; control quantities **b** $\Delta g^n_{\rm SJ}$ and **c** $\Delta g^n_{\rm UD}$ corresponding to detector and beam line asymmetries which cancel in quadruple ratio, and their comparison to MC

The inefficiency of the LKr component of the L1N trigger was measured with a sample of minimum bias triggers. It amounted to 0.7% in supersamples I and II, and 3% in supersamples III and IV. For supersamples V, VI and VII the L1N condition was relaxed to compensate for the above degradation by adding in "OR" a condition requiring the total LKr energy deposition to exceed 15 GeV to the initial condition based on the presence of at least two clusters, which resulted in a stable inefficiency of 0.03%. The degradation of the trigger performance at the beginning of supersample III was later identified to be due to a small time misalignment between parts of the hardware trigger logic.

The inefficiency of the LKr component of L1N is a priori charge symmetric, since it is based on LKr energy deposit conditions. To confirm this, the inefficiency has been studied using a MC simulation, with an LKr map of local trigger inefficiency (measured directly from the data) used as a reference. Several checks have been performed, in particular by artificially increasing the measured inefficiency or by including totally inefficient regions. No systematic effects have been observed at a level of $\delta(\Delta g^n) = 0.1 \times 10^{-4}$, which is considered a systematic uncertainty due to the LKr component of the L1 trigger.

The inefficiency of the L2N trigger was mostly due to local inefficiencies of the DCHs, and varied from 4% to 6%. The effects due to such inefficiencies, being of geometrical nature, have been simulated by a MC. No charge asymmetry was found; upper limits of systematic uncertainties from other (smaller) possible effects, including those related to variations of timing offsets between subdetectors and data buffer overflows, were estimated directly by variation of the selection conditions. The total systematic uncertainty induced by L2N inefficiency was estimated not to exceed $\delta(\Delta g^n) = 0.3 \times 10^{-4}$.

5.5 Other systematic effects

Effects related to the magnetic spectrometer do not affect the result significantly, since the charged track is only used for the identification of the kaon charge and in the mass cut. In particular, systematic effects due to spectrometer misalignment (see Sect. 4.2), momentum scale (see Sect. 4.3), and geometrical acceptance for the charged track (see Sect. 4.4), which are important issues for the analysis in the $K^\pm \to 3\pi^\pm$ mode, were found to be negligible for the $K^\pm \to \pi^\pm\pi^0\pi^0$ analysis.

Uncertainties related to imperfect knowledge of the permanent magnetic field in the decay volume were found not to exceed $\delta(\Delta g^n) = 0.1 \times 10^{-4}$ by artificially varying the field map in accordance with the precision of its measurement. Stability of the result with respect to variation of the selected $\pi^\pm\pi^0\pi^0$ invariant mass interval was checked, and no systematic deviation was found.

Systematic uncertainty due to the difference of K^+ and K^- production spectra was conservatively estimated in the same way as for the $K^\pm \to \pi^\pm\pi^+\pi^-$ mode (described in Sect. 4.7), and found to be $\delta(\Delta g^n) = 0.3 \times 10^{-4}$.

Systematic uncertainties due to event pile-up were found not to exceed $\delta(\Delta g^n) = 0.2 \times 10^{-4}$ by varying the selection conditions on the allowed extra activity in the detectors, and by checking the stability of the result with respect to the timing cuts.

Charge-asymmetric material effects, which are negligible, were discussed in Sect. 4.7.

5.6 The resulting A_g^n

The systematic uncertainties are summarized in Table 6. The difference in the linear slope parameters of K^+ and

Table 6. Systematic uncertainties on the measured value of Δg^n

Systematic effect	Uncertainty $\delta(\Delta g^n) \times 10^4$
Overlap of LKr showers	±0.5
L1 HOD trigger inefficiency	±0.1
L1 LKr trigger inefficiency	±0.1
L2 trigger inefficiency	±0.3
Stray magnetic fields	±0.1
Kaon production spectra	±0.3
Pile-up	±0.2
Total systematic uncertainty	±0.7

K^- decays into $\pi^\pm\pi^0\pi^0$ was measured with the full NA48/2 data sample of 9.13×10^7 events to be

$$\Delta g^n = (2.2\pm2.1_{\rm stat.}\pm0.7_{\rm syst.})\times10^{-4}\,. \qquad (11)$$

The corresponding direct CP violating asymmetry (3) obtained using the nominal value of the linear slope parameter $g^n = 0.626\pm0.007$ [13] is

$$A_g^n = (1.8\pm1.7_{\rm stat.}\pm0.6_{\rm syst.})\times10^{-4} = (1.8\pm1.8)\times10^{-4}\,. \qquad (12)$$

The uncertainties of the measured A_g^c and A_g^n are similar, despite a ratio of the sample sizes of $N^c/N^n = 34$. The main reason for compensation of the difference in sample sizes is a small ratio of the linear slope parameters of the two decay modes: $|g^c/g^n| = 0.34$.

6 Discussion of the results

The measurement of Δg differences between the linear Dalitz plot slopes was chosen as a representative quantity of a possible direct CP violation effect, and is the quantity on which most theoretical and experimental investigations are focused. In absence of a specific model for physics beyond the SM it is not possible to state in general terms which difference in K^+ and K^- decay distributions is expected to give the most significant CP violating effect.

Discussing the asymmetry of linear slopes, it should be remarked that the recent discovery by NA48/2 [37] (and theoretical interpretation [14–16]) of the distortion of the $\pi^\pm\pi^0\pi^0$ Dalitz plot distribution due to final state interactions between pions indicated the need for alternative parameterizations. Rescattering terms can be conveniently accommodated into a parameterization based on a polynomial expansion of the decay amplitude itself (rather than the event density) which, for the non-rescattering part, would be:

$$|M'(u,v)|^2 \sim (1+g'u/2+h'u^2/2+k'v^2/2+\ldots)^2\,. \qquad (13)$$

The relation between the slope parameters appearing in (1) and (13) is, at first order, $g'=g$, $h'=h-g^2/4$, $k'=k$. Measurement of $\Delta g'$ in the framework of the parameterization (13) involves fitting of the quadruple ratio of measured u distributions (5) with a function

$$f'(u) = n\cdot\left(1+\frac{\frac{1}{2}\Delta g' u}{1+\frac{1}{2}g'u+\frac{1}{2}h'u^2}\right)^8\,, \qquad (14)$$

rather than (6).

The results of the measurement of Δg in the framework of parameterizations (1) and (13) were compared. The result in the $K^\pm\to3\pi^\pm$ mode is stable within 0.1×10^{-4}, and its error is insensitive to the parameterization. On the other hand, the result in the $K^\pm\to\pi^\pm\pi^0\pi^0$ mode obtained with (13) is

$$\Delta g' = (3.2\pm3.1_{\rm stat.})\times10^{-4}\,, \qquad (15)$$

to be compared with (11). The significant variation of the central value and its error is mostly due to the relatively large values of the slope parameters g^n and h^n. Introduction of the additional $\pi\pi$ rescattering term to the amplitude (13) does not considerably change the result with respect to (15).

The sensitivity discussed above is one of the reasons to publish the tabulated quadruple ratios along with the results of the fits.

7 Conclusions

NA48/2 has measured the charge asymmetries of Dalitz plot linear slopes in both three-pion $K^\pm$ decay modes to be

$$A_g^c = (-1.5\pm2.2)\times10^{-4},\quad A_g^n = (1.8\pm1.8)\times10^{-4}, \qquad (16)$$

which is an improvement in accuracy over the previous measurements [13] by more than one order of magnitude. NA48/2 precisions are limited mainly by the available statistics.

The measured asymmetries do not show evidences for large enhancements due to non-SM physics. They are consistent with the SM predictions, in particular with a full next-to-leading order ChPT calculation [18] predicting

$$A_g^c = (-1.4\pm1.2)\times10^{-5},\quad A_g^n = (1.1\pm0.7)\times10^{-5}\,. \qquad (17)$$

Due to the high precision achieved, the results can be used to constrain extensions of the SM predicting enhancements of the CP violating effects.

Acknowledgements. It is a pleasure to thank the technical staff of the participating laboratories, universities and affiliated computing centres for their efforts in the construction of the NA48 apparatus, in the operation of the experiment, and in the data processing.

References

1. J.H. Christenson et al., Phys. Rev. Lett. **13**, 138 (1964)
2. NA31 Collaboration, H. Burkhardt et al., Phys. Lett. B **206**, 169 (1988)
3. NA31 Collaboration, G. Barr et al., Phys. Lett. B **317**, 233 (1993)
4. NA48 Collaboration, V. Fanti et al., Phys. Lett. B **465**, 335 (1999)
5. NA48 Collaboration, A. Lai et al., Eur. Phys. J. C **22**, 231 (2001)
6. NA48 Collaboration, J.R. Batley et al., Phys. Lett. B **544**, 97 (2002)
7. KTeV Collaboration, A. Alavi-Harati et al., Phys. Rev. Lett. **83**, 22 (1999)
8. KTeV Collaboration, A. Alavi-Harati et al., Phys. Rev. D **67**, 012 005 (2003)
9. Babar Collaboration, B. Aubert et al., Phys. Rev. Lett. **87**, 091 801 (2001)

10. Belle Collaboration, K. Abe et al., Phys. Rev. Lett. **87**, 091 802 (2001)
11. Belle Collaboration, K. Abe et al., Phys. Rev. Lett. **93**, 021 601 (2004)
12. Babar Collaboration, B. Aubert et al., Phys. Rev. Lett. **93**, 131 801 (2004)
13. PDG Collaboration, W.-M. Yao et al., J. Phys. G **33**, 1 (2006)
14. N. Cabibbo, Phys. Rev. Lett. **93**, 121 801 (2004)
15. N. Cabibbo, G. Isidori, JHEP **0503**, 021 (2005)
16. G. Colangelo et al., Phys. Lett. B **638**, 187 (2006)
17. G. Isidori, L. Maiani, A. Pugliese, Nucl. Phys. B **381**, 522 (1992)
18. E. Gámiz, J. Prades, I. Scimemi, JHEP **10**, 042 (2003)
19. G. Fäldt, E. Shabalin, Phys. Lett. B **635**, 295 (2006)
20. E.P. Shabalin, ITEP preprint **8-98** (1998)
21. G. D'Ambrosio, G. Isidori, G. Martinelli, Phys. Lett. B **480**, 164 (2000)
22. W.T. Ford et al., Phys. Rev. Lett. **25**, 1370 (1970)
23. K.M. Smith et al., Nucl. Phys. B **91**, 45 (1975)
24. TNF–IHEP Collaboration, G.A. Akopdzhanov et al., Eur. Phys. J. C **40**, 343 (2005)
25. NA48/2 Collaboration, J.R. Batley et al., Phys. Lett. B **634**, 474 (2006)
26. NA48/2 Collaboration, J.R. Batley et al., Phys. Lett. B **638**, 22 (2006)
27. Y. Giomataris et al., Nucl. Instrum. Methods A **376**, 29 (1996)
28. B. Peyaud et al., Nucl. Instrum. Methods A **535**, 247 (2004)
29. D. Bèderéde et al., Nucl. Instrum. Methods A **367**, 88 (1995)
30. G.D. Barr et al., Nucl. Instrum. Methods A **370**, 413 (1996)
31. NA48 Collaboration, V. Fanti et al., Nucl. Instrum. Methods A **574**, 433 (2007)
32. NA48/2 Collaboration, J.R. Batley et al., Phys. Lett. B **649**, 349 (2007)
33. GEANT Description and Simulation Tool, CERN Program Library Long Writeup **W5013**, (1994)
34. R. Frühwirth, Nucl. Instrum. Methods A **262**, 444 (1987)
35. J.R. Cudell et al., Phys. Rev. D **65**, 074 024 (2002)
36. NA48/2 Collaboration, H.W. Atherton et al., CERN 80-07
37. J.R. Batley et al., Phys. Lett. B **633**, 173 (2006)